AGU ADVANCING EARTH AND SPACE SCIENCE

Water Resources Research

RESEARCH ARTICLE
10.1029/2021WR031403

The Effect of Large Wood Accumulations With Rootwads on Local Geomorphic Changes

D. Ravazzolo[1,2], G. Spreitzer[1,3], J. Tunnicliffe[4], and H. Friedrich[1]

[1]Department of Civil and Environmental Engineering, University of Auckland, Auckland, New Zealand, [2]Mediterranean Ecogeomorphological and Hydrological Connectivity Research Team, Department of Geography, University of the Balearic Islands, Palma, Spain, [3]Laboratory of Hydraulics, Hydrology and Glaciology (VAW), ETH Zurich, Zurich, Switzerland, [4]School of Environment, University of Auckland, Auckland, New Zealand

Key Points:

- Large wood with rootwads generates more stable large wood accumulations than large wood without rootwads
- The presence of rootwads leads to the formation of more loosely packed large wood accumulations, resulting in higher porosity
- Large wood accumulations with rootwads lead to a slight increase in geomorphic changes compared to accumulations without rootwads

Correspondence to:
D. Ravazzolo,
d.ravazzolo@uib.es

Citation:
Ravazzolo, D., Spreitzer, G., Tunnicliffe, J., & Friedrich, H. (2022). The effect of large wood accumulations with rootwads on local geomorphic changes. *Water Resources Research*, *58*, e2021WR031403. https://doi.org/10.1029/2021WR031403

Received 7 NOV 2021
Accepted 11 MAY 2022

Abstract Large wood (LW) can be transported along a river during floods, increasing flood-associated hazards, particularly when it accumulates at river-spanning infrastructures such as bridges and weirs. While most flume studies have explored LW movement with simple wooden elements (dowels), only a few studies have used elements with more complex LW geometries, such as rootwads, under unsteady flow conditions. Quantitative assessment of interactions amongst more complex wood elements and river flow has rarely been attempted the effect of this additional complication has even been ignored, in both field and laboratory studies. In this study, flume experiments were conducted to assess the effect of rootwads on local scour and deposition in a flume with a mobile gravel-bed. The experiment was conducted under unsteady flow conditions, with a constricted segment of the reach, recreating conditions to wood accumulations and blockage. Results revealed that LW with rootwads tends to generate more stable accumulations than LW without rootwads, leading to the formation of more porous loosely packed accumulations. In this initial set of flume experiments, the patterns of scour were quite variable, but on average, the porous and stable LW accumulations with rootwads showed more spatially extensive disturbance of the bed. LW accumulations without rootwads led to the development of scour pits that reached the bottom of the flume more quickly than in the LW accumulations without rootwads. The mean accumulated bedload volumes were of similar magnitude overall, however, highlighting the many contingencies in the chain of processes between dam formation and resultant bed scour.

Plain Language Summary When instream wood accumulates at river-crossing infrastructure (e.g., bridges and weirs), complex flow-sediment-wood interactions take place. Various shapes of logs typically make up those accumulations, such as logs with and without branches and rootwads, with the different shapes having a contrasting influence on local bed morphology (i.e., local sediment scour and deposition). While most flume studies have explored log movements by using simple wooden elements (dowels), only a few studies have used complex log geometries under unsteady flow conditions. In this study, we experimentally assess the effects of rootwads on bed morphology in a mobile gravel-bed flume, upstream of a bridge. The experiment was conducted under unsteady flow conditions, recreating conditions that have been found to lead to wood accumulation formation. The results indicate that logs with rootwads generate more stable (i.e., few dowels bypassed the accumulation) and porous wood accumulations than accumulations without rootwads. Wood accumulations of logs with rootwads influence the local flow field, developing, over a wider area, more extended morphological changes than wood accumulations without rootwads. Such findings provide important information for stream managers but also have important implications to improve future river-spanning infrastructure design.

1. Introduction

Large wood (LW) is recruited into river systems either through incremental or chronic processes, such as attributed to tree mortality and bank undercutting, or through episodic processes (i.e., flood events, landslides, windthrow, debris flows, and wildfire; Bisson et al., 1987; Keller & Swanson, 1979; Wohl et al., 2012). Once in channel, LW provides many benefits to riverine ecological communities, enhancing the quantity and quality of in-stream habitats and physical (i.e., morphological and hydraulic) diversity of river systems (Collins & Montgomery, 2002; Gurnell et al., 2002; Maser & Sedell, 1994). LW can affect channel form and morphological processes by increasing or decreasing bank stability (Montgomery et al., 2003) or influencing the development of bars in braided rivers (Bertoldi et al., 2013; Mao et al., 2020). Marston (1982) reported that the amount of sediment retained by

LW can be higher than 100% of the total annual bedload yield in third-order to fifth-order streams. Moreover, sediment retention and associated geomorphic effects (i.e., local sediment scour and deposition) vary depending on the structure and size of the LW element or LW jam (LWJ) along the channel network (Abbe & Montgomery, 2003; Keller & Swanson, 1979). Large quantities of LW may be mobilized during high-magnitude flows, introducing potential hazards for humans (Ravazzolo et al., 2017) and infrastructure (Comiti et al., 2012; Lucía et al., 2015; Mazzorana et al., 2009; Rigon et al., 2012). The mobilization of large quantities of LW can cause extensive damage along the channel network, mainly because of LWJs at bridges and weirs (Steeb et al., 2017) that might trigger hazardous channel avulsions (Comiti et al., 2008; Marchi et al., 2009).

Laboratory experiments are well-suited to better study and capture the complex interactions between LW, sediment, flow, and infrastructure (Friedrich et al., 2021). However, physical modeling of LW processes that explicitly considers complex and realistic shapes still presents unexplored challenges. The earliest laboratory studies focused on LW accumulations at bridge piers, and their subsequent influence on the flow. One of the earliest experiments, conducted by Laursen and Toch (1956), showed qualitatively that LW accumulation can affect flow velocities, resulting in deeper and more extensive bed scour. Melville and Dongol (1992) observed that flow velocity, sediment size and a pier's shape and upstream orientation relative to the flow direction are governing parameters in the process of scour. Subsequently, flume experiments conducted by Lagasse et al. (2010) showed that accumulation porosity and roughness have only a minor effect on the resulting local scour, compared to the size, shape, and location of the LWJ body. Pagliara and Carnacina (2010) assessed the temporal scour evolution and morphology for different LW roughness and porosity conditions. Their study showed that the upstream-facing area of the blockage is the main parameter that affects the resulting bed scour. Combined geomorphic and hydraulic impacts of LW in a sand bed channel were explored in a flume experiment by Wallerstein et al. (2001). They observed that the size of constituent LW elements was the governing parameter for the magnitude of scour. More recent investigations associated local scour with rising backwater effects, due to LWJs. Schalko et al. (2018, 2019a) reported that the maximum local scour due to LW accumulations is mainly governed by the unit discharge, mean grain size diameter, and the LW volume required to trigger the main backwater rise. Our literature review revealed that physical modeling is often the only way to systematically refine our understanding of cause and effect at different spatial and temporal scales in an otherwise complex and often dangerous field environment. By simplifying complex objects' shapes (e.g., mimicking LW with cylindrical dowels), physical modeling allows us to simplify and capture processes occurring in rivers, which are otherwise rarely, if ever, measured in the field.

LW has more complex geometrical characteristics besides length and diameter, influencing their entrainment, trapping, and flow-blocking potential. Fresh LW elements tend to have branches and rootwads that greatly affect transport and depositional behavior. The presence of rootwads or branches can inhibit LW movement by anchoring pieces to the riverbed, increasing drag and decreasing mobility (Abbe & Montgomery, 1996; Bisson et al., 1987; Buxton, 2010; Welber et al., 2013). During low flow conditions, rootwads may project downward and elevate LW, reducing the submerged volume and thus the buoyancy and hydrodynamic drag (Braudrick & Grant, 2000). Thus, the presence or absence of rootwads can be indicative of the relative stability and function of LW accumulations (Abbe et al., 1997; Braudrick & Grant, 2000). Indeed, Merten et al. (2010), documenting the characteristics and locations of 865 natural wood pieces in nine streams in Minnesota, reported that wooden elements with rootwads were associated with a lower probability of mobilization. Additionally, Benda and Bigelow (2014) reported that trees recruited by bank erosion, which include rootwads and branches, typically have a greater geomorphic influence on streams. Iroumé et al. (2018) also observed that unrooted LW is prone to travel longer distances than LW with attached rootwads, confirming studies by Abbe and Montgomery (1996) and Cadol and Wohl (2010). The anchoring effects of LW with rootwads in morphologically and hydraulically unstable locations are thus of great relevance for channel morphological processes and the safety of engineered structures (Davidson et al., 2015).

Although it has been demonstrated that rootwads can influence LW volume and mobility, quantitative assessment of their effect is rarely addressed, and is even ignored, in both field and laboratory experiments (Wohl et al., 2010). Among the few studies that have been conducted so far, Schmocker and Hager (2011) demonstrated that, under steady flow conditions, the blocking probability for both simple logs and logs with rootwads decreases with an increasing Froude number. Schalko et al. (2021) highlighted the negligible importance of LW shape (e.g., rootwads and branches) on both backwater rise and bedload retention. Welber et al. (2013) explored the characterization of LW deposition patterns, linked to LW characteristics (e.g., rootwads), flow rate, and bed

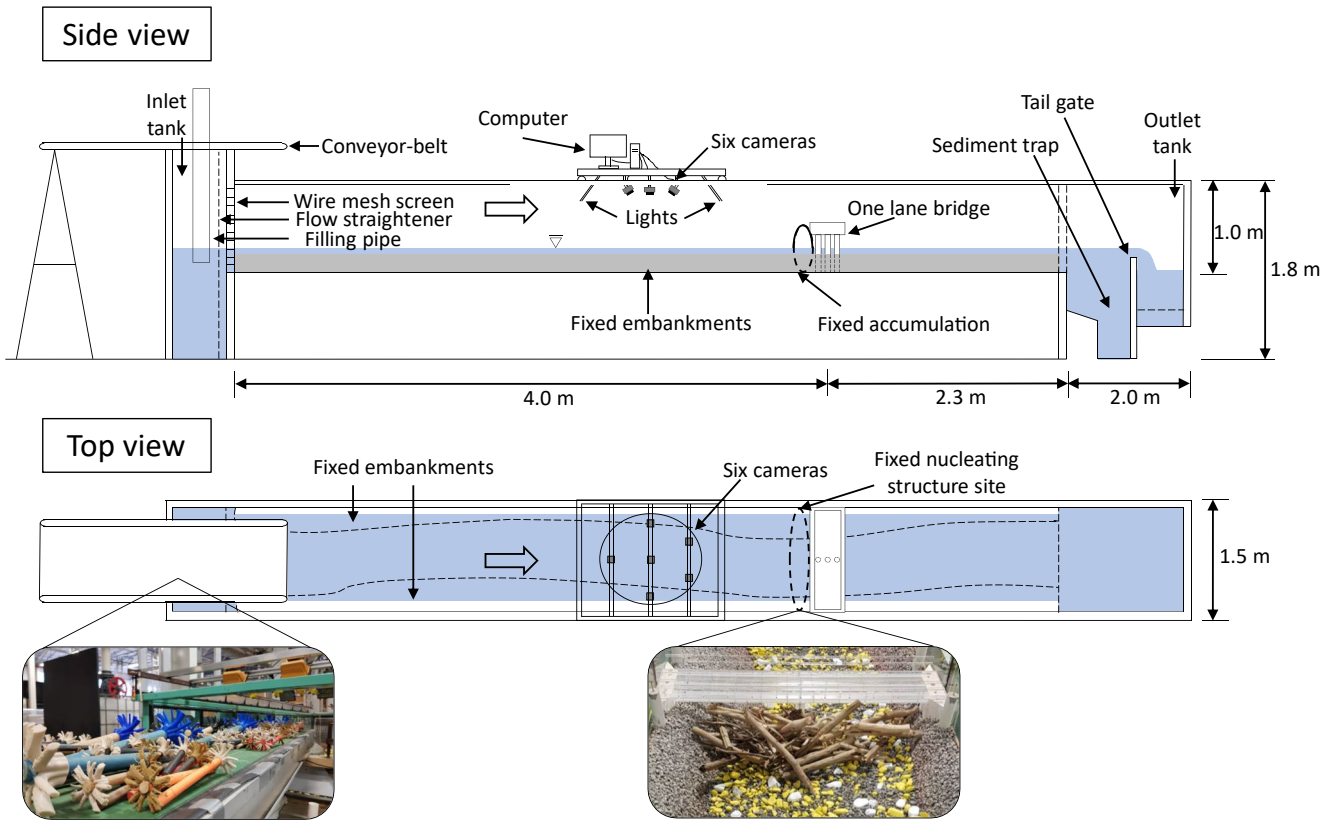

Figure 1. Experimental setup, illustrating side and top view of the flume, the employed fixed LW accumulation upstream of the bridge structure, and dowels with rootwads.

morphology. There remains much to be learned about sediment-flow-wood interactions under unsteady flow conditions.

In this study, a flume experiment was conducted to assess the effects of rootwads on local scour and deposition in a mobile gravel-bed flume, upstream of a constricted cross-section. The experiment was conducted under unsteady flow conditions, recreating conditions that have been found to lead to LWJ formation, offering new insights into the interaction between flow, sediment, and LW. The resultant geomorphic changes of the flume bed were evaluated using Structure-from-Motion (SfM) photogrammetry, confirming the technique's potential to provide valuable quantitative insight into wood-influenced river hydraulics and morphodynamics, as demonstrated in previous studies (i.e., Spreitzer et al., 2021; Al-Zawaidah et al., 2021). Additionally, we explore the effects of rootwads on LW transport dynamics and travel velocity during flood events. Understanding wood transport dynamics and characterizing interactions between LW and bed morphology is crucial for improving the design of river-spanning infrastructure subjected to direct and indirect impacts from LWJs. The present study also demonstrates how LW with rootwads may influence LWJ emplacement (e.g., shape, volume, and stability) and resultant changes to river morphology.

2. Materials and Methods

2.1. Flume Characteristics

The flume experiment was conducted in a 6.3 m-long, 1.5 m-wide, and 1 m-deep flume in the Water Engineering Laboratory at the University of Auckland. The flume was configured to reproduce a characteristic New Zealand upland gravel-bed river, scaled at a ratio of 1:15 (Figure 1). The river was gently sinuous, with a bed slope of 0.02. The bed and fixed banks were lined with a thin sublayer of concrete. The inclined embankment surface was covered with a cemented granular layer, with grains ranging in diameter from 8 to 16 mm, to impart the

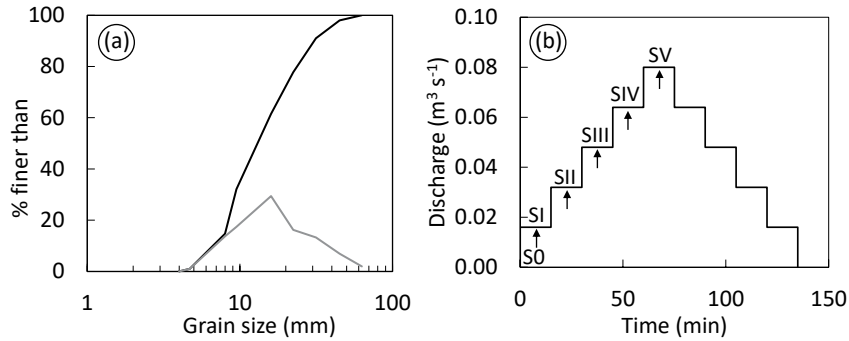

Figure 2. Grain size distribution of the sediment mixture (a); stepped hydrograph simulation in five steps (S0–SV). The black arrows correspond to the LW input.

appropriate hydraulic roughness. A flow straightener was used at the inlet to minimize excess turbulence. Along the 6.3-m long flume, the active channel's width ranged from 0.8 to 1 m. A mixture of water-worked sediment truncated at 4 mm (finest) and 45 mm (coarsest), with $D_{16} = 8.1$ mm, $D_{50} = 13$ mm, and $D_{84} = 26.3$ mm was used as bed material. Bed material was manually mixed and then screeded homogenously along the entire channel to reach a thickness of approximately 0.07 m. Sediment output was collected using a filtering bedload trap placed at the downstream end of the flume.

Flow rates were controlled via an electromagnetic valve and unit discharges ranged from 6 to 80 $l \cdot s^{-1}$. The experiment used a stepped hydrograph, designed to represent a bankfull flood event for the prototype catchment (an area of about 100 km^2). The hydrographs, composed of nine steps, were symmetrical about the peak discharge, each with a duration of 15 min (Figure 2). Four meters downstream from the inlet, a one-lane bridge with a row of piers oriented in stream-wise direction was placed in the center of the channel. The bridge was a scaled, representation of a 22.5-m long and 3.6-m wide, single-lane rural bridge. To avoid major flushing of the full depth of the active bed layer in the reach of the bridge structure (extending from 1 m upstream of the bridge to the downstream end of the flume), the mechanical roughness of the thin concreted sublayer was increased by installing the same cement-granular mixture as used for the embankments. Thus, the physical model resembles a mobile bed layer over broken bedrock fragments that can be temporarily exposed under extreme conditions. To easily distinguish the fixed channel bed from the mobile bedload layer during the experiments, the fixed sublayer of the bed was painted red.

2.2. Wooden Dowels and Wood Accumulations

A total of 193 cylindrical wooden dowels were supplied from a custom-designed conveyor-belt system above the inlet structure. The LW input consisted of a mixture of eight different dowel sizes, ranging from 10 to 25 mm in diameter and 100 to 400 mm in length. The wood had a uniform density of 0.5 $g \cdot cm^{-3}$, similar to logs used by Braudrick and Grant (2001), Gschnitzer et al. (2017), and Spreitzer et al. (2019). In addition, the density corresponded to that of *Pinus radiata*, a commercial timber species that is widely planted in New Zealand. The total volume supplied in each experimental run was approximately 0.006 m^3 (6 L), representing an LW volume of 300 m^3. The addition of rootwads increased the net wood volume by approximately 0.0015 m^3. This is reasonably consistent with the scaling of event-based observations of LW yield at retention structures and bridges (for a catchment of 100 km^2), deposited along streams, and retained in reservoirs and lakes (Ruiz-Villanueva et al., 2016).

To enable the formation of LWJs at the bridge, a fixed nucleating structure was built using rigid pieces of natural wood collected from the field. These wood components ranged from 0.1 to 0.4 m in length and 0.01 to 0.25 m in diameter. Screws and wire were used to assemble the LW accumulation structure, before it was placed upstream of the bridge piers. This design has been used successfully in previous LW studies (Ravazzolo et al., 2020; Spreitzer et al., 2018, 2021).

2.3. Rootwad Modeling

A *P. radiata* rootwad model was designed using Blender, an open-source mesh modeling and animation software (v. 2.91; www.blender.org). The major roots were trimmed to make the overall morphology consistent with a root mass that has been broken and abraded after some transit time in the river. The model design was exported to ".stl" format (abbr. from stereolithography) and imported to Ultimaker Cura software (v. 4.9; software for 3D printer control). MeshLab (v. 2016.12) was used to scale different rootwad sizes to fit dowel dimensions. Subsequently, the rootwad models were printed with a Creality CR-10S5 3D printer, using the common Polylactic Acid (PLA) filament for 3D printer. PLA has a density of about 1.24 g·cm^{-3}. With the application of infill material, the resulting rootwads had a density of roughly 0.5 to 0.7 g·cm^{-3}, similar to the density of the wooden dowels. Finally, the cylindrical dowels were plugged into the 3D printed rootwad models. The greater volume of the rootwad affected the dowel's floating balance, projecting it downward and increasing its submerged volume, as described in Braudrick and Grant (2000).

2.4. Video Recording and Camera Array Setup for the SfM Photogrammetry Technique

Three GoPro Hero 6 video cameras were employed to capture the motion of the LW elements (Ravazzolo et al., 2017; Ruiz-Villanueva et al., 2019). One GoPro was installed above the flume's inlet, with a view downstream, and a second was installed above the outlet, looking upstream. The third GoPro was fixed on the righthand glass wall to record LW dynamics and the evolution of the LWJs over time. VideoPad video editor by NCH software (v. 10.60) was used to analyze the footage frame by frame. The images collected were also imported in ArcMap (v. 10.5) to analyze the orientation of individual dowels with respect to the flow direction, as well as to assess the shape of LWJs. SfM photogrammetry was carried out using a six-camera array mounted on a mobile carriage above the flume channel. The cameras had a 5.5-mm lens with 13-megapixel CMOS image sensor. Five cameras were mounted in a pentagon arrangement, with a 0.25-m distance between them, inclined at an angle of 15°, all oriented toward the central ground point. A center camera was mounted with nadir orientation, also focused on the central ground point.

As the carriage was moved in steps of 0.1 m along the longitudinal axis of the flume, images of the bed were collected from a constant elevation of 0.8 m. Full coverage of the stream reach entailed a total of 282 images, resulting in image overlap of approximately 80%. Similar coverage between images was successfully used in previous studies (Ravazzolo et al., 2020; Spreitzer et al., 2018). Control recording time (i.e., the time between the pictures) and camera parameters (e.g., contrast, brightness, and exposure) of image acquisition were set using a software algorithm in Visual Studio Code (v. 147). Ground control points for point cloud model alignment were collected using a SokkiaTotal Station CX 105. Agisoft Metashape (v. 1.7.1) software was used to generate point clouds from the overlapping images. The point clouds were then imported into ArcMap (v. 10.5), where Digital Elevation Models (DEMs) of the bed elevation were generated (cell size 1.5 × 1.5 mm^2) and detrended. DEMs from surveys collected before and after each run (DEMpre and DEMpost, respectively) were used to generate DEMs of difference (hereafter DoD; = DEMpost − DEMpre). The DoDs were finally thresholded to a change detection level of ±0.02 m, to account for uncertainty arising from noise in the change model. This scaling is consistent with guidelines for photogrammetry surveys proposed by Wheaton et al. (2013), and deployed in the Geomorphic Change Detection (GCD) software (http://gcd.joewheaton.org). The GCD interface was used to analyze the patterns of volumetric erosion and deposition. Furthermore, the point cloud models were meshed in Agisoft Metashape and transferred to Autodesk Meshmixer (v. 3.5.474), where a fully closed 3D body of each LWJ was generated and assessed for its total volume (V_{tot}), according to the method introduced by Spreitzer et al. (2020a). The percentage of porous space (n) of each LWJ was calculated by the volumetric proportion of V_{tot} and the known net volume of wood (V_w) componing the LWJ (i.e., nucleating structure, rootwads, and dowels componing the LWJ), using Equation 1:

$$n = \frac{V_{tot} - V_w}{V_{tot}} * 100\,(\%) \quad (1)$$

Table 1
Experimental Test Program

Experimental run	Number of repetitions	Timeline	Measurement
RF	1	A: Base flow	–
		B: Stop pump	SfM1
		C: Run	–
		D: Stop pump	SfM2
LW − R	4	A: Base flow	–
		B: Stop pump	SfM3
		C: Run + Dowel input	
		D: Remove dowels	Dowel count + SfM4
LW + R	4	A: Base flow	–
		B: Stop pump	SfM5
		C: Run + Dowel input	
		D: Remove dowels	Dowel count + SfM6

2.5. Experimental Procedure

To capture the variation in patterns of local geomorphic change (local erosion and deposition) and to assess the effect of packing density and complexity in LWJs, two different scenarios were simulated: an LWJ composed of LW elements with rootwads (LW + R), and without rootwads (LW − R). Four experimental runs were conducted for each scenario. In addition, one experimental run was conducted without any dowel supply (RF), and this served as a reference bed state for the models that had dowels (Table 1). The RF run was conducted with the nucleating structure in place.

After setting up the channel bed, a natural bed structure was allowed to evolve under a base flow of 6 $l \cdot s^{-1}$ for 20 hr in each experimental run. At the end of the initiation period, bed topography was surveyed using SfM photogrammetry. In each experimental run, the flow rate was gradually increased until it reached a discharge of 16 $l \cdot s^{-1}$ for 15 min. Five groups of wooden dowels (for both scenarios LW − R and LW + R) were placed on a conveyor-belt. Each group was composed of the same number and size of dowels (0.0012 m^3 of wood per each group). Wood dowels were supplied via the conveyor-belt halfway through each step in the hydrograph during the rising limb(four steps plus the peak; Figure 2b) in a congested regime (Braudrick et al., 1997). The LW + R were introduced with rootwads facing upstream, as this has been shown to be the typical transport orientation for trees during floods (Francis et al., 2008).

At the end of each experimental run, the channel was drained, dowels were manually removed without disturbing the channel bed, and image acquisition for SfM photogrammetry was conducted. Water levels were measured during the experimental runs at three gauging stations before and after the introduction of LW. The stations were spaced at 1-m intervals; two stations were upstream of the bridge, and the third was downstream (Figure 2). The dowels were counted at the end of the experimental runs, and sediment yielded from the run was recovered from the outlet sediment trap. Then, it was sieved into three size groups (small—from 4 to 8 mm, medium—from 8 to 16 mm, and large—from 16 to 45 mm), and weighted.

2.6. Statistical Analysis

Since data were not normally distributed, the nonparametric Kruskal-Wallis statistical test was applied. The test allowed us to explore differences between groups. Differences were considered statistically significant for a p-value < 0.05. All statistics were performed using IBM SPSS statistics (v. 26; IBM Corp., 2019).

3. Results

3.1. LW Transport and LWJ Dynamics

In both scenarios, 193 LW elements (with or without rootwads) were supplied to the active channel from the most upstream part of the flume. With the introduction of LW − R, on average, 65% of the total dowels remained trapped at the fixed nucleating structure and developed LWJs. In contrast, the introduction of the LW + R resulted in 85% retention of all supplied LW. Of the bypassing dowels, almost 71% of LW − R and 90% of LW + R elements were of the smallest size range (0.01 m in diameter and 0.1 m in length). Dowels of larger size were thus most likely to be trapped. During step V of the hydrograph (peak flow; Figure 2b), the jam lost its ability to retain new dowels, and in both LW − R and LW + R runs, newly introduced elements largely tended to bypass the LWJs.

From the video footage it was observed that dowels of both LW − R and LW + R were mainly transported parallel to the flow direction during steps I, II, and III. This behavior changed in steps IV and V, when dowels were more likely to travel in a random orientation relative to the flow. Dowels without rootwads traveled at a higher velocity than those with rootwads in all steps. This was particularly evident during step I, where LW + R recorded a median velocity of 0.55 $m \cdot s^{-1}$, lower than LW − R, which traveled at a median velocity of 0.94 $m \cdot s^{-1}$. The breakdown of LW flow velocities is shown in Figure 3. Generally, dowels without rootwads interacted with other

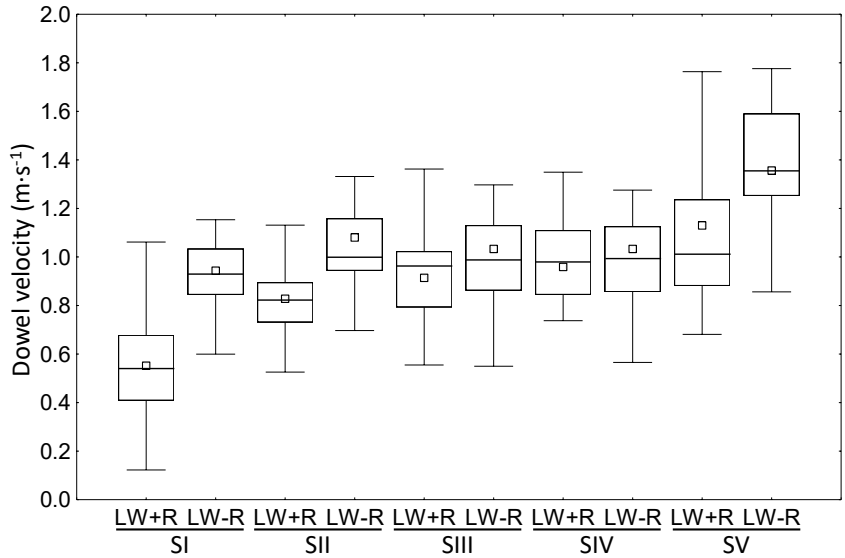

Figure 3. Dowel velocity during discharge steps I, II, III, IV, and V of the hydrograph for LW − R and LW + R experimental runs. The horizontal line and square within each box indicate the mean and median values. Box boundaries represent 25th and 75th percentiles, and whiskers indicate the minimum and maximum velocities observed.

pieces during transit, but did not yaw from side to side during their transport. Dowels with rootwads were likely to be transported in a more random orientation relative to the flow direction and exhibited a greater tendency to yaw. The videos revealed that the smallest dowels with rootwads were the only elements likely to travel with a flow-parallel orientation, especially during the hydrograph peak, showing the lowest median velocity of 1.1 m·s^{-1}. The results of the Kruskal-Wallis test supported the inference that there was a statistical significance between LW + R and LW − R in steps I, II, and V (p-value < 0.05). No statistical significance was found in steps III and IV (p-value > 0.05).

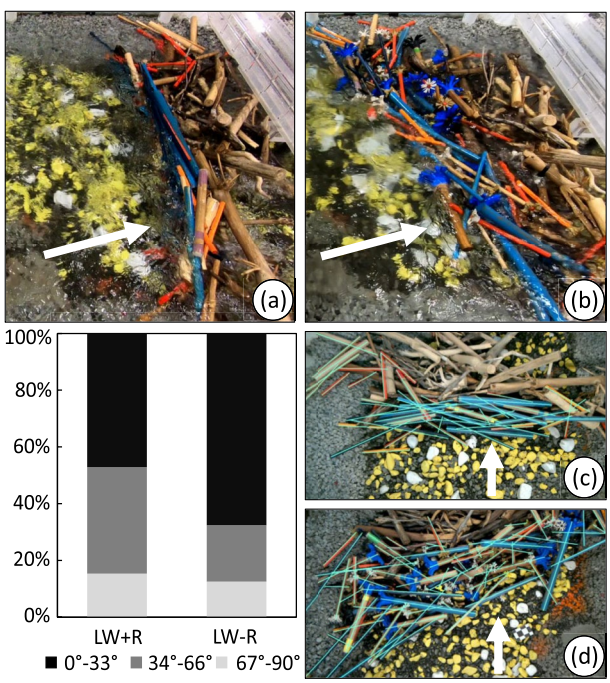

Figure 4. LWJs at the peak of the hydrograph (step V), for both LW − R (a) and LW + R (b) experimental runs. The graph indicates dowel orientation relative to the main flow direction for both LW − R and LW + R experimental runs, obtained from ArcMap analysis. Compact (a, c) and looser (b, d) packing of the LW − R and LW + R jams (respectively) was observed. The white arrows indicate the main flow direction.

Once trapped at the LWJs, video footage revealed that both LW − R and LW + R elements were likely to amass in a random orientation relative to the flow direction at peak flood stage. In contrast, the dowels tended to accumulate perpendicularly to the main flow direction at lower flows. Qualitatively, the final shape of the LW − R jams appeared to be more compact and aligned, with almost 25% more dowels oriented from 0° to 33° relative to the main flow direction than those formed by LW + R elements (Figure 4). Indeed, as indicated in Figure 5, the porosity of LW + R LWJs ranged between 58% and 68%. In contrast, porosity ranged between 47% and 56% for LW − R LWJs. The median porosity was lower for LW − R (51%) than LW + R (62.5%). According to the Kruskal-Wallis test, these differences were statistically significant (p-value < 0.05).

3.2. Effect of LWJs on Backwater Rise

As dowels were retained at the fixed nucleating structure site, a growing backwater profile was observed in both (LW − R and LW + R) experimental runs (Figure 6). On average, a similar rise (during the rising limb) and fall (during the falling limb) of the water surface profile was observed: 0.012 m for LW − R and 0.013 m for LW + R. However, during LW + R a median elevation differential of 0.004 m was observed between rising and falling limbs ($\Delta h_{ris} - \Delta h_{fal}$), which was lower than the 0.020 m measured during LW − R experimental runs (Figure 6b). The results of the Kruskal-Wallis

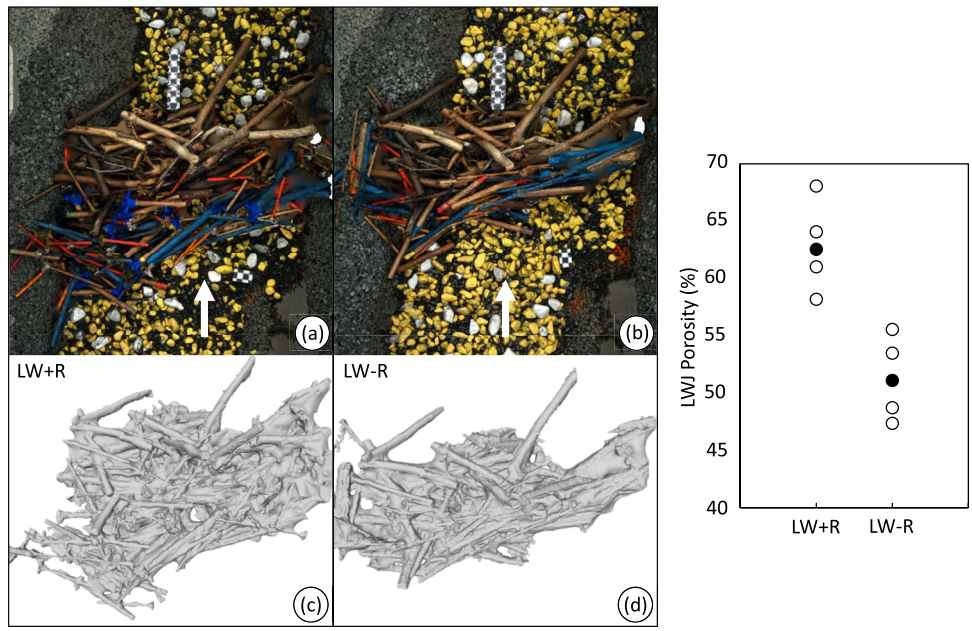

Figure 5. Examples of generated DEM models in Agisoft Metashape (a, b), and fully closed 3D bodies of the corresponding LWJs (c, d). The white arrows indicate the main flow direction. The graph on the right side indicates porosity parameters obtained for LWJs with and without rootwads at the end of each experimental run. The black dots represent the median value for all runs in both sequences.

test on these differentials did not reveal any statistically significant difference between the LW + R and LW − R populations (p-value > 0.05).

3.3. Effect of LWJs on Local Geomorphic Changes

Although geomorphic changes were observed for the RF run, no bed material arrived at the sediment trap. In contrast, once the LWJs began to form at the critical cross-section, confined flow and higher bed shear stress resulted in more pronounced entrainment of the bed material and corresponding geomorphic change. Figure 7 shows the fractional yield quantities for the three grain size categories (plus the total), for both LW − R and LW + R scenarios. In all groups, LW − R experienced a wider range of sediment transport intensities than LW + R. However, the median values were lower for LW − R than LW + R. On average, 25.8% of the total gravel

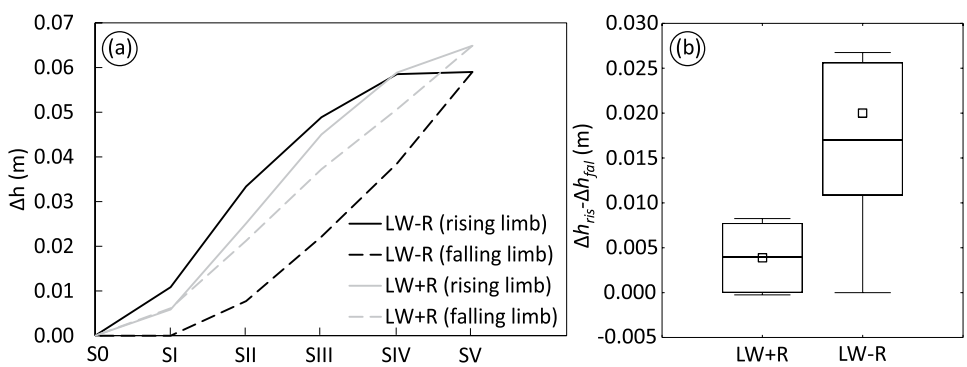

Figure 6. (a) Backwater rise (Δh) during rising (solid lines) and falling limb (dotted lines) of the different steps (S0–SV) of the hydrograph, for both LW − R (black line) and LW + R (gray line). (b) Difference between the backwater rise during the rising (Δh_{ris}) and falling (Δh_{fal}) limbs of the different steps (S0–SV) of the hydrograph, for both LW − R and LW + R experimental runs. The lines and squares within each box indicate the mean and median values, while box boundaries represent 25th and 75th percentiles. The whiskers indicate the minimum and maximum values.

10.1029/2021WR031403

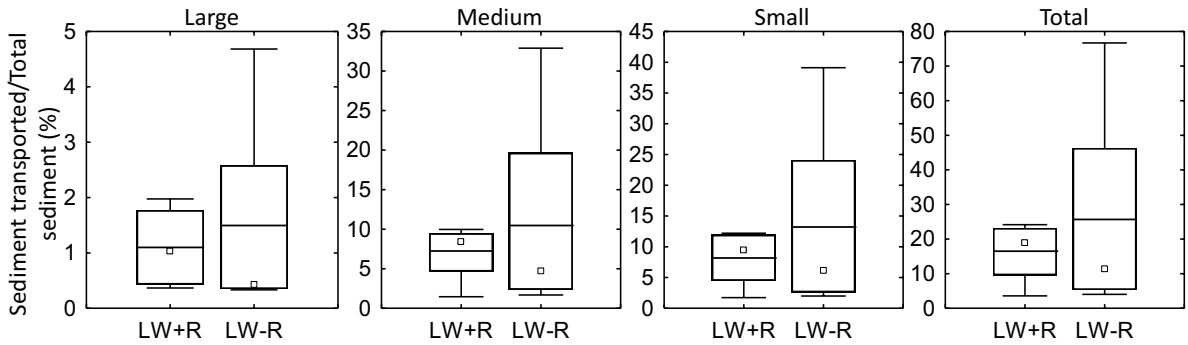

Figure 7. Sediment transport partitioned by gravel size groups (small—from 4 to 8 mm, medium—from 8 to 16 mm, and large—from 16 to 45 mm), and the total sediment arriving at the outlet trap at the end of both LW + R and LW − R experimental runs. The square and the horizontal line within each box indicate the median and mean values. Box ends are 25th and 75th percentiles, and whiskers are the minimum and maximum values.

material available accumulated in the sediment trap at the end of the LW − R experimental runs (horizontal line within the boxes of LW − R in Figure 7), and 16.4% at the end of LW + R experimental runs (horizontal line within the boxes of LW + R in Figure 7). The median of the total quantity of sediment transported was 6.8 kg for LW − R and 11.3 kg for LW + R. According to the Kruskal-Wallis test, these resulting median values in the LW + R and LW − R scenarios were not statistically different (p-value > 0.05).

The volume and spatial extent of geomorphic change were evaluated using the DoDs (Figure 8). Quantitative assessment of change volumes was carried out using the GCD tool in ArcMap (Figure 9). The minimum change detection noise threshold for the difference model was determined to be 0.02 m. The volume in this region of uncertainty averaged about 15% for the total volume change that was assessed in the difference model. The errors were found to be at an acceptable level to ensure appropriate geomorphic change assessment. Some minor deformation of the reconstructed surface manifested as a result of rounded-vault-distortion of the flat surface, also known as "doming." This is a distortion artifact commonly encountered in photogrammetric surveys. For all runs, no significant changes were observed in the upstream part of the flume. Changes were evident at the

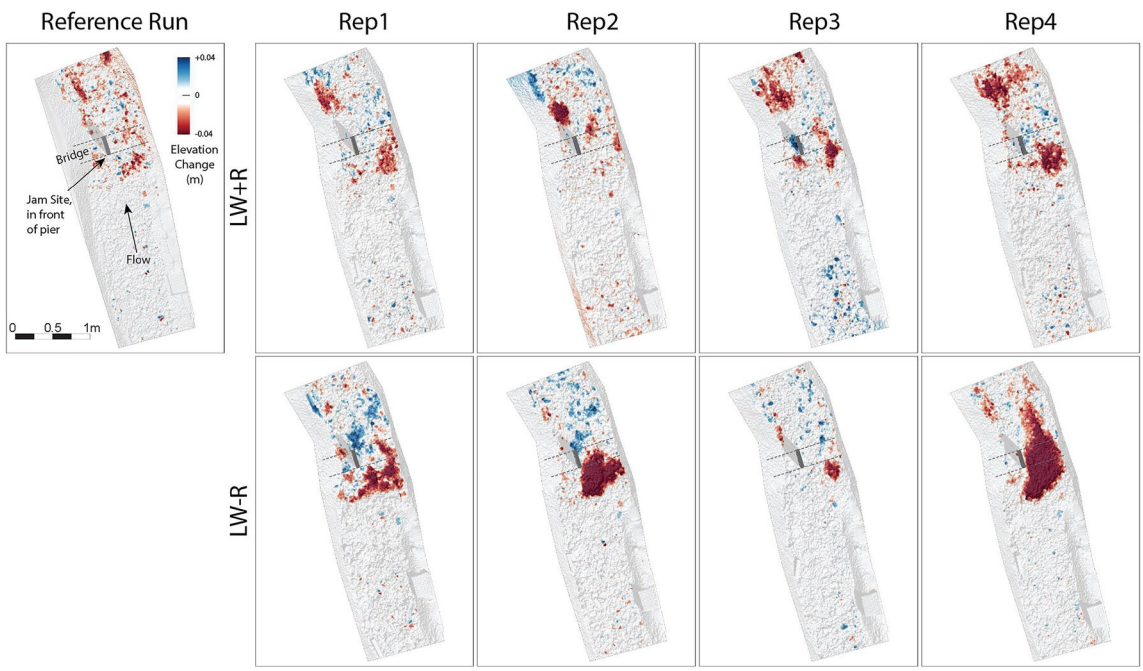

Figure 8. DEM of Difference (DoDs) for both LW + R and LW − R experimental runs.

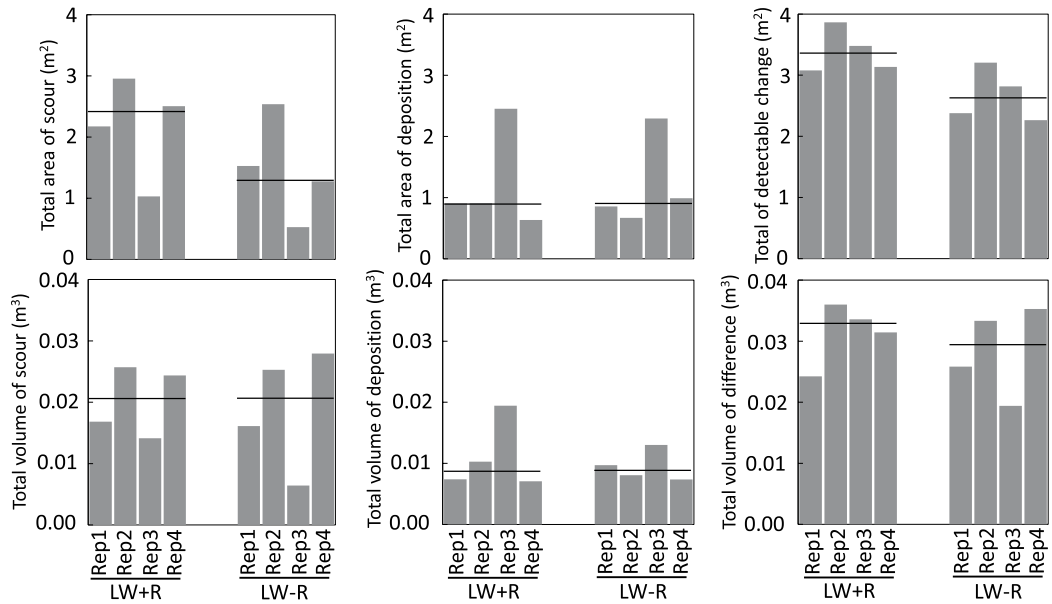

Figure 9. Summary of geomorphic change results obtained for both LW − R and LW + R experimental runs, using the Geomorphic Change Detection (GCD) tool. Horizontal lines within each group of repetitions correspond to the repetitions' median value.

critical cross-section, near the LWJs, and downstream of them. Scour (red color in Figure 8) resulted in the most pronounced geomorphic change detected in LW − R and LW + R experimental runs.

In terms of the total scour area, LW + R experimental runs showed a greater median value (2.3 m^2) than LW − R (1.4 m^2). A similar extent of erosion (~0.9 m^2) was calculated in both LW − R and LW + R (Figure 9). The total area of detectable geomorphic changes was higher in LW + R (3.3 m^2) than in LW − R (2.6 m^2). Although a greater scour area was observed for LW + R, the median scour volume (~0.02 m^3) was similar for both runs. Similar median values were also obtained for the deposition volume (~0.009 m^3). Overall, a slightly higher median volume of net geomorphic change was reported for LW + R (0.033 m^3) than for LW − R (0.03 m^3), with the small difference attributed to the occasional exposure of the concreted sublayer for LW − R only experimental runs, otherwise the absence of rootwads could have led to a slightly larger difference. In accordance, LW − R showed the largest range in scour volume (Figure 9), occasionally exposing the modeled bedrock.

4. Discussion

4.1. The Effect of Rootwads on LW Dynamics

To date, laboratory investigations into the LW dynamics of rootwads have primarily been conducted using individual pieces, ignoring the effects of interactions between LW elements (e.g., Braudrick & Grant, 2000; Shields & Alonso, 2012; Wallerstein et al., 2001). Although rootwads are recognized as having an important influence on LW dynamics, little quantitative information on their role is found in the literature. So far, most laboratory studies have used simple cylindrical dowels, with limited exploration of more complex LW geometries and compositional variation of jam components. However, devising more sophisticated experimental arrangements is essential to better understand the entrainment of LW elements and accumulation, persistence, and dispersal of LWJs. Rootwads can decrease the travel velocity of LW (as reported by Abbe & Montgomery, 1996; Braudrick & Grant, 2000) and they have been found to significantly influence dowel motion at low flows (Welber et al., 2013). Our experiments confirm these earlier findings, as we observed a significant difference between LW + R and LW − R velocities in the initial (steps I and II) and in the maximum (step V) hydrograph stages. Additionally, we demonstrate that LW components with rootwads travel more slowly and tend to settle in a more random arrangement with respect to flow direction, than simple cylinders. This more random structural alignment of LW + R elements was found to affect LWJ packing porosity, as well as compression and relaxation effects of

wood assemblages in the flow (Spreitzer et al., 2021), altering flow hydraulics (backwater effects) and channel morphology differently with respect to LWJs of LW − R. Rootwads significantly alter the LW center of mass. The heavier rootwad end will drag on the channel bottom, increasing frictional resistance and, in turn, decreasing the travel velocity during transport. In addition to this drag, there was evident pivoting or yawing of LW + R components during travel, again resulting in a decrease of transport velocity. Similar observations on the relatively more efficient transit of LW − R have been made by Abbe and Montgomery (1996), Braudrick and Grant (2000), and Bocchiola et al. (2006). In this experiment, a relatively simple, single-thread channel morphology was selected. Generally, LW with rootwads is less likely to become anchored in such U-shaped channels; mid-channel bars, point bars, and side-channels, for instance, offer greater opportunity for grounding. The effect is quite pronounced in braided lowland rivers, where bars tend to trap LW (Gurnell et al., 2002; Ravazzolo, Mao, Picco, & Lenzi, 2015; Ravazzolo, Mao, Picco, Sitzia, et al., 2015). We observed that once LW was introduced into the flume channel, it accumulated at the critical cross-section, with a consequent increase in backwater level, as has been observed in several recent studies, such as Schalko et al. (2018, 2019a), Al-Zawaidah et al. (2021), and Spreitzer et al. (2021). Although LWJs with rootwads were found to retain a higher number of arriving dowels, thus increasing LWJ volume, the resulting higher LWJ porosity presented less of an obstacle to flow than did the LWJs without rootwads. This, in turn, results in a similar backwater profile gradient during the rising and falling limb of the hydrograph. In the absence of rootwads, the LW elements were more likely to bypass the bridge, resulting in different backwater levels between the rising and falling limb. In both LW + R and LW − R experimental runs, it was determined that the backwater profile diminished rapidly once bed scour was initiated, similar to observations by Schalko et al. (2019b) and Al-Zawaidah et al. (2021). We further hypothesize that different processes (e.g., pivoting of logs and different settling) occurring simultaneously might lead to different backwater effects, instigated by LW + R or LW − R. For example, a different retained accumulation volume, the shape of the LWJ and thus the porosity can affect the local scour, resulting in different backwater rise. Therefore, other factors should be further investigated with larger datasets to obtain statistically significant regression models.

4.2. The Effect of Rootwads on Reach Morphodynamics

This laboratory experiment has shown that in both scenarios (LW + R and LW − R), an LWJ large enough to interact with local bedload transport developed. LWJs contributed to the modification of bed characteristics and channel morphology. This aligns with our knowledge that jams can generate hydraulic roughness and drag (Gippel, 1995) that trigger local scour and sediment deposition around a bridge's piers. The DoDs obtained from the simulated flood event show a discontinuous sediment transport pathway along the river reach. In both scenarios, sediment was most likely to be mobilized under the LWJs and a short distance downstream, as previously observed by Spreitzer et al. (2021). While the total mobilized bedload volume observed in Figure 9 was similar for runs with LW − R and LW + R, there was a notable difference in the spatial distribution of this erosion. Schalko et al. (2019b) and Al-Zawaidah et al. (2021) observed that scour increases when flow increases. However, at the highest flows, when the stability of the jam begins to falter, the ability of the LW + R to trap more dowels with its complex form ensures greater LWJ longevity. In addition, the presence of rootwads led to increased LWJ porosity (i.e., void spaces), which, in turn, influenced the local flow fields. The porosity generated more turbulent flow conditions in the downstream reach of the LWJs, which may have led to the slightly greater variability in bed scour characteristics for the LW + R runs. The perpendicular orientation of the LW − R dowels created a less porous obstruction, leading to flow diversion and a visually evident supercritical flow condition below the LWJ, focusing the scour area and mobilizing a wider range of coarser sediment (Figure 7). LWJs in the LW − R experimental runs led to the development of scour pits that reached the bottom of the flume more quickly than in the LW + R runs. Schalko et al. (2019b) observed similar rapid local scouring processes using homogeneous sediment. Porosity of the LWJs was therefore deemed to be a key factor in shaping of the flow field by LWJs (e.g., Al-Zawaidah et al., 2021; Manners & Doyle, 2008; Manners et al., 2007; Spreitzer et al., 2020b; Spreitzer et al., 2021). This kind of flow alteration and its characteristics should be investigated more closely: we hypothesize that tight and aligned LW elements, rather than the studied jam of randomly distributed structural alignment of the elements, will enhance bed scour even further. Although the results support our observations, the relationship is not statistically strong. This demonstrates that there are many contingencies in the process of jam construction, and thus the number of replications needed to ensure statistically significant results should be suitably high. To develop a more robust relationship between the geometry of the woody elements and scour

induced by jams, more runs could be carried out, perhaps varying other boundary conditions such as channel form and the nature of the constriction.

4.3. Implications and Perspectives for Future Experiments

Our study demonstrates how our understanding of the complex wood-sediment-flow interactions during LWJ formation can be effectively explored using laboratory experimental techniques. Since wood-sediment-flow interactions have not been extensively explored, there are several opportunities for further study to increase our understanding of such interactions.

Discharge variability and timing. In our experiment, we simulated a symmetrical stepped hydrograph, mimicking a flood event with flow restrained by banks. Future physical models should explore hydraulic and geomorphological interactions, employing more realistic hydrographs, with different shapes or sequences of hydrographs. According to Gurnell et al. (2000), a larger volume of LW is generally stored after major flood events. Therefore, when discharge increases, LW quantity and transport also tend to increase (MacVicar & Piégay, 2012). However, future studies should also consider flood timing and seasonality, as they govern vegetational growth (Greet et al., 2011; Mahoney & Rood, 1998), and thus influence LW availability, quantity, and characteristics (e.g., density, geometry, and size).

LWJ characteristics (e.g., porosity and density). To the authors' knowledge, there are no studies investigating the flow response in the presence of different porosities and flow scenarios. Thus, the hydraulic influence of LWJs can change as porosity and LWJ size vary over time. We believe it is an essential need to develop more realistic and case-specific flow models in the presence of LWJs. As demonstrated in the present study, LWJ's porosity may be the main factor in modifying the local bed roughness and channel morphology, with likely a consequence on bedforms' distribution.

A large piece of dense wood is less mobile than a similar-sized piece of lower density. In the present experiment, we used dowels of the same density. Wood density varies widely depending on tree species but also according to water content and degree of decay. We advocate that variation in the buoyancy characteristics of wood in transit might strongly affect jam formation, and the relative porosity of the resultant structure. Work by Al-Zawaidah et al. (2021) demonstrated that LWJs of different densities generate different patterns and volumes of local scour. More studies should be conducted combining different LW characteristics, such as more complex LW geometries with varying specific weight parameters.

LW features. The use of a 3D printer allowed us to reproduce the rootwad form of a specific tree species. Future experimental work should further leverage this technology to explore LW behavior with different features (e.g., trunk and rootwad shape, branches) and different stiffness levels.

Evolution of micro and macro-morphology of channel bed. In this study, the SfM photogrammetry technique generated satisfactory models of channel topography, achieving a resolution of less than half of the diameter of the smallest grain fraction employed in the channel. The creation and disintegration of bed sedimentary microforms, upstream and downstream of the critical cross-section, should be considered in future studies. We show again how appropriate physical models can be a useful tool for studying the temporal evolution of geomorphic processes. SfM photogrammetry has demonstrated enormous potential for time-lapse 4D assessment (Eltner & Sofia, 2020).

5. Conclusions

Flume experiments were conducted to study the effect of LWJs with rootwads on local geomorphic changes within a mobile gravel substrate at a constricted cross-section. Results show that LW elements with rootwads generate more stable LWJs than elements without rootwad. The presence of rootwads leads to greater stability and more complex LWJ shape, resulting in fewer LW elements that can bypass during a modeled flood event. Because of the structural resilience of LWJs with rootwads, similar backwater levels were observed during the rising and falling limbs of the hydrograph. In addition, the present study reveals that dowels with rootwads tend to form more loosely packed accumulations, resulting in significantly higher LWJ porosity than observed for LWJs without rootwads. The increased porosity, combined with the LWJs' greater stability, influences the strengths

of the local flow field, generating geomorphic changes across a wider area than those caused by LWJs without rootwads.

The results summarized here provide valuable information for stream managers, as it has been demonstrated that LWJs at a critical cross-section can modify the channel morphology differently, depending solely on the presence or absence of rootwads. Furthermore, these findings have important implications for future experimental research related to the understanding of wood transport dynamics and characterizing interactions between LW and bed morphology. This work can improve the design of river-spanning infrastructure subjected to LWJs, as well as the design and installation of engineered log jams for river restoration projects. Given the high damage potential at critical cross-sections due to LWJ emplacement during floods, further studies should be conducted to better understand the complex interactions amongst wood, sediment, and flow around such infrastructure.

Data Availability Statement

Data generated and used in this study are available online (https://figshare.com/s/db095d4313d734f07958), as well as provided in the presented tables and figures.

Acknowledgments
The authors would like to thank Matthew Wang and Nathan Browne for helping during the experiments. Danny Baucke and Charlotte Milne are thanked for helping with the generation of the DEMs and DoDs. The authors thank the technical staff at the Water Engineering Laboratory of the University of Auckland for their support. Thanks also to the anonymous reviewers and Editor Ellen Wohl for their helpful comments on earlier drafts of this manuscript.

References

Abbe, T. B., & Montgomery, D. R. (1996). Large woody debris jams, channel hydraulics, and habitat formation in large rivers. *Regulated Rivers: Research & Management*, *12*, 201–221. https://doi.org/10.1002/(SICI)1099-1646(199603)12:2/3<201::AID-RRR390>3.0.CO;2-A

Abbe, T. B., & Montgomery, D. R. (2003). Patterns and processes of wood debris accumulation in the Queets river basin, Washington. *Geomorphology*, *51*(1–3), 81–107. https://doi.org/10.1016/S0169-555X(02)00326-4

Abbe, T. B., Montgomery, D. R., & Petroff, C. (1997). Design of stable in-channel wood debris structures for bank protection and habitat restoration: An example from the Cowlitz River, WA. In S. S. Y. Wang, E. J. Langendoen, & F. D. Shields (Eds.), *Management of landscapes disturbed by channel incision: Stabilization, rehabilitation, restoration* (pp. 809–815). University of Mississippi.

Al-Zawaidah, H., Ravazzolo, D., & Friedrich, H., (2021). Local geomorphic effects in the presence of accumulations of different densities. *Geomorphology*, *389*, 107838. https://doi.org/10.1016/j.geomorph.2021.107838

Benda, L., & Bigelow, P. (2014). On the patterns and processes of wood in northern California streams. *Geomorphology*, *209*, 79–97. https://doi.org/10.1016/j.geomorph.2013.11.028

Bertoldi, W., Gurnell, A. M., & Welber, M. (2013). Wood recruitment and retention: The fate of eroded trees on braided river explored using a combination of field and remotely-sensed data sources. *Geomorphology*, *180–181*, 145–155. https://doi.org/10.1016/j.geomorph.2012.10.003

Bisson, P. A., Bilby, R. E., Bryant, M. D., Dolloff, C. A., Grette, G. B., House, R. A., et al. (1987). Large woody debris in forested streams in the Pacific Northwest: Past, present, and future. In E. O. Salo & T. W. Cundy (Eds.), *Streamside maznagement: Forestry and fishery interactions* (pp. 143–190). University of Washington, Institute of Forest Resources Contribution No. 57.

Bocchiola, D., Rulli, M. C., & Rosso, R. (2006). Flume experiments on wood entrainment in rivers. *Advances in Water Resources*, *29*(8), 1182–1195. https://doi.org/10.1016/j.advwatres.2005.09.006

Braudrick, C. A., & Grant, G. E. (2000). When do logs move in rivers? *Water Resources Research*, *36*, 571–583. https://doi.org/10.1029/1999wr900290

Braudrick, C. A., & Grant, G. E. (2001). Transport and deposition of large woody debris in streams: A flume experiment. *Geomorphology*, *41*(4), 263–283. https://doi.org/10.1016/S0169-555X(01)00058-7

Braudrick, C. A., Grant, G. E., Ishikawa, Y., & Ikeda, H. (1997). Dynamics of wood transport in streams: A flume experiment. *Earth Surface Processes and Landforms*, *22*(7), 669–683. https://doi.org/10.1002/(SICI)1096-9837(199707)22:7<669::AID-ESP740>3.0.CO;2-L

Buxton, T. H. (2010). Modeling entrainment of waterlogged large wood in stream channels. *Water Resources Research*, *46*, W10537. https://doi.org/10.1029/2009WR008041

Cadol, D., & Wohl, E. (2010). Wood retention and transport in tropical, headwater streams, La Selva Biological Station, Costa Rica. *Geomorphology*, *123*(1–2), 61–73. https://doi.org/10.1016/j.geomorph.2010.06.015

Collins, B. D., & Montgomery, D. R. (2002). Forest development, wood jams, and restoration of floodplain rivers in the Puget Lowland, Washington. *Restoration Ecology*, *10*(2), 237–247. https://doi.org/10.1046/j.1526-100X.2002.01023.x

Comiti, F., D'Agostino, V., Moser, M., Lenzi, M. A., Bettella, F., Dell'Agnese, A., et al. (2012). *Preventing wood-related hazards in mountain basins: From wood load estimation to designing retention structures*. Paper presented at the 12th Interpraevent Congress, Grenoble, France (pp. 651–662).

Comiti, F., Mao, L., Preciso, E., Picco, L., Marchi, L., & Borga, M. (2008). Large wood and flash floods: Evidences from the 2007 event in the Davča basin (Slovenia). In D. De Wrachien, M. A. Lenzi, & C. A. Brebbia (Eds.), *Monitoring, simulation, prevention and remediation of dense and debris flow II* (pp. 173–182). WIT-Press.

Davidson, S. L., Mackenzie, L. G., & Eaton, B. C. (2015). Large wood transport and jam formation in a series of flume experiments. *Water Resources Research*, *51*, 10065–10077. https://doi.org/10.1002/2015WR017446

Eltner, A., & Sofia, G. (2020). Structure from motion photogrammetric technique. In *Developments in Earth surface processes* (pp. 1–24). https://doi.org/10.1016/b978-0-444-64177-9.00001-1

Francis, R. A., Tibaldeschi, P., & McDougall, L. (2008). Fluvially-deposited large wood and riparian plant diversity. *Wetlands Ecology and Management*, *16*, 371–382. https://doi.org/10.1007/s11273-007-9074-2

Friedrich, H., Ravazzolo, D., Ruiz-Villanueva, V., Schalko, I., Spreitzer, G., Tunnicliffe, J., & Weitbrecht, V. (2021). Physical modelling of large wood (LW) processes relevant for river management: Perspectives from New Zealand and Switzerland. *Earth Surface Processes and Landforms*, 1–26. https://doi.org/10.1002/esp.5181

Gippel, C. J. (1995). Environmental hydraulics of large woody debris in streams and rivers. *Journal of Environmental Engineering*, *121*(5), 388–395. https://doi.org/10.1061/(ASCE)0733-9372(1995)121:5(388)

Greet, J., Angus Webb, J., & Cousens, R. (2011). The importance of seasonal flow timing for riparian vegetation dynamics: A systematic review using causal criteria analysis. *Freshwater Biology*, *56*(7), 1231–1247. https://doi.org/10.1111/j.1365-2427.2011.02564.x

Gschnitzer, T., Gems, B., Mazzorana, B., & Aufleger, M. (2017). Towards a robust assessment of bridge clogging processes in flood risk management. *Geomorphology*, *279*, 128–140. https://doi.org/10.1016/j.geomorph.2016.11.002

Gurnell, A. M., Petts, G. E., Hannah, D. M., Smith, B. P., Edwards, P. J., Kollmann, J., et al. (2000). Wood storage within the active zone of a large European gravel-bed river. *Geomorphology*, *34*(1), 55–72. https://doi.org/10.1016/S0169-555X(99)00131-2

Gurnell, A. M., Piegay, H., Swanson, F. J., & Gregory, S. V. (2002). Large wood and fluvial processes. *Freshwater Biology*, *47*, 601–619. https://doi.org/10.1046/j.1365-2427.2002.00916.x

IBM Corp. Released. (2019). *IBM SPSS statistics for Windows, version 26.0*. IBM Corp.

Iroumé, A., Ruiz-Villanueva, V., Mao, L., Barrientos, G., Stoffel, M., & Vergara, G. (2018). Geomorphic and stream flow influences on large wood dynamics and displacement lengths in high gradient mountain streams (Chile). *Hydrological Processes*, *32*, 2636–2653. https://doi.org/10.1002/hyp.13157

Keller, E., & Swanson, F. J. (1979). Effects of large organic material on channel form and fluvial processes. *Earth Surface Processes and Landforms*, *4*, 361–380.

Lagasse, P. F., Clopper, P. E., Zevenbergen, L. W., Spitz, W. J., & Girard, L. G. (2010). *Effects of debris on bridge pier scour* (NCHRP Rep. 653). Washington, D. C: Transportation Research Board. Retrieved from http://onlinepubs.trb.org/onlinepubs/nchrp/nchrp_rpt_653.pdf

Laursen, E. M., & Toch, A. (1956). Scour around bridge piers and abutments (*Bulletin No. 4*). Iowa Highway Research Board. Iowa Institute of Hydraulic Research in cooperation with the Iowa State Highway Commission and the Bureau of Public Roads, IA, USA.

Lucía, A., Comiti, F., Borga, M., Cavalli, M., & Marchi, L. (2015). Dynamics of large wood during a flash flood in two mountain catchments. *Natural Hazards and Earth System Sciences*, *15*, 1741–1755. https://doi.org/10.5194/nhess-15-1741-2015

MacVicar, B., & Piégay, H. (2012). Implementation and validation of video monitoring for wood budgeting in a wandering piedmont river, the Ain River (France). *Earth Surface Processes and Landforms*, *37*, 1272–1289. https://doi.org/10.1002/esp.3240

Mahoney, J. M., & Rood, S. B. (1998). Streamflow requirements for cottonwood seedling recruitment—An integrative model. *Wetlands*, *18*, 634–645. https://doi.org/10.1007/BF03161678

Manners, R. B., & Doyle, M. W. (2008). A mechanistic model of woody debris jam evolution and its application to wood-based restoration and management. *River Research and Applications*, *24*, 1104–1123. https://doi.org/10.1002/rra.1108

Manners, R. B., Doyle, M. W., & Small, M. J. (2007). Structure and hydraulics of natural woody debris jams. *Water Resources Research*, *43*(6), 1–17. https://doi.org/10.1029/2006WR004910

Mao, L., Ravazzolo, D., & Bertoldi, W. (2020). The role of vegetation and large wood on the topographic characteristics of braided river systems. *Geomorphology*, *367*, 107299. https://doi.org/10.1016/j.geomorph.2020.107299

Marchi, L., Borga, M., Preciso, E., Sangati, M., Gaume, E., Bain, V., et al. (2009). Comprehensive post-event survey of a flash flood in Western Slovenia: Observation strategy and lessons learned. *Hydrological Processes*, *23*(26), 3761–3770. https://doi.org/10.1002/hyp.7542

Marston, R. A. (1982). The geomorphic significance of log steps in forest streams. *Annals of the American Association of Geographers*, *72*, 99–108. https://doi.org/10.1111/j.1467-8306.1982.tb01386.x

Maser, C., & Sedell, J. R. (1994). *From the forest to the sea. The ecology of wood in streams, rivers, estuaries, and oceans*. Delray Beach: St Lucie Press. https://doi.org/10.2307/1467738

Mazzorana, B., Zischg, A., Largiader, A., & Hübl, J. (2009). Hazard index maps for woody material recruitment and transport in alpine catchments. *Natural Hazards and Earth System Sciences*, *9*(1), 197–209. https://doi.org/10.5194/nhess-9-197-2009

Melville, B. W., & Dongol, D. M. (1992). Bridge pier scour with debris accumulation. *Journal of Hydraulic Engineering*, *118*(9), 1306–1310. https://doi.org/10.1061/(ASCE)0733-9429(1992)118:9(1306)

Merten, E., Finlay, J., Johnson, L., Newman, R., Stefan, H., & Vondracek, B. (2010). Factors influencing wood mobilization in streams. *Water Resources Research*, *46*, W10514. https://doi.org/10.1029/2009WR008772

Montgomery, D. R., Collins, B. D., Buffington, J. M., & Abbe, T. B. (2003). Geomorphic effects of wood in rivers. In S. V. Gregory, K. L. Boyer, & A. M. Gurnell (Eds.), *The ecology and management of wood in world rivers (American Fisheries Society Symposium 37)* (pp. 21–47). American Fisheries Society.

Pagliara, S., & Carnacina, I. (2010). Temporal scour evolution at bridge piers: Effect of wood debris roughness and porosity. *Journal of Hydraulic Research*, *48*(1), 3–13. https://doi.org/10.1080/00221680903568592

Ravazzolo, D., Mao, L., Mazzorana, B., & Ruiz-Villanueva, V. (2017). Brief communication: The curious case of the large wood-laden flow event in the Pocuro stream (Chile). *Natural Hazards and Earth System Sciences*, *17*, 2053–2058. https://doi.org/10.5194/nhess-2017-154

Ravazzolo, D., Mao, L., Picco, L., & Lenzi, M. A. (2015). Tracking log displacement during floods in the Tagliamento River using RFID and GPS tracker devices. *Geomorphology*, *228*, 226–233. https://doi.org/10.1016/j.geomorph.2014.09.012

Ravazzolo, D., Mao, L., Picco, L., Sitzia, T., & Lenzi, M. A. (2015). Geomorphic effects of wood quantity and characteristics in three Italian gravel-bed rivers. *Geomorphology*, *246*, 79–89. https://doi.org/10.1016/j.geomorph.2015.06.012

Ravazzolo, D., Spreitzer, G., Friedrich, H., & Tunnicliffe, J. (2020). Flume experiments on the geomorphic effects of large wood in gravel-bed rivers. In *Proceedings of river flow 2020* (pp. 1609–1615). CRC Press.

Rigon, E., Comiti, F., & Lenzi, M. A. (2012). Large wood storage in streams of the Eastern Italian Alps and the relevance of hillslope processes. *Water Resources Research*, *48*, W01518. https://doi.org/10.1029/2010WR009854

Ruiz-Villanueva, V., Mazzorana, B., Mao, L., Ravazzolo, D., Wohl, E., Burkli, L., et al. (2019). Characterization of wood-laden flows in rivers. *Earth Surface Processes and Landforms*, *44*, 1694–1709. https://doi.org/10.1002/esp.4603

Ruiz-Villanueva, V., Piégay, H., Gurnell, A. M., Marston, R. A., & Stoffel, M. (2016). Recent advances quantifying the large wood dynamics in river basins: New methods and remaining challenges. *Reviews of Geophysics*, *54*, 611–652. https://doi.org/10.1002/2015RG000514

Schalko, I., Lageder, C., Schmocker, L., Weitbrecht, V., & Boes, R. M. (2019a). Laboratory flume experiments on the formation of spanwise large wood accumulations: I. Effect on backwater rise. *Water Resources Research*, *55*(6), 4854–4870. https://doi.org/10.1029/2019WR024789

Schalko, I., Lageder, C., Schmocker, L., Weitbrecht, V., & Boes, R. M. (2019b). Laboratory flume experiments on the formation of spanwise large wood accumulations: Part II—Effect on local scour. *Water Resources Research*, *55*(6), 4871–4885. https://doi.org/10.1029/2019WR024789

Schalko, I., Ruiz-Villanueva, V., Maager, F., & Weitbrecht, V. (2021). Wood retention at inclined bar screens: Effect of wood characteristics on backwater rise and bedload transport. *Water*, *13*, 2231. https://doi.org/10.3390/w13162231

Schalko, I., Schmocker, L., Weitbrecht, V., & Boes, R. M. (2018). Backwater rise due to large wood accumulations. *Journal of Hydraulic Engineering*, *144*, 04018056. https://doi.org/10.1061/(ASCE)HY.1943-7900.0001501

Schmocker, L., & Hager, W. H. (2011). Probability of drift blockage at bridge decks. *Journal of Hydraulic Engineering*, *137*, 470–479. https://doi.org/10.1061/(ASCE)HY.1943-7900.0000319

Shields, F. D., & Alonso, C. V. (2012). Assessment of flow forces on large wood in rivers: Lift and drag on large wood. *Water Resources Research*, *48*, W04516. https://doi.org/10.1029/2011WR011547

Spreitzer, G., Friedrich, H., & Tunnicliffe, J. (2018). Effects of a large woody debris accumulation on channel-bed morphology during flood events. *E3S Web of Conferences*, *40*, 02024. https://doi.org/10.1051/e3sconf/20184002024

Spreitzer, G., Gibson, J., Tang, M., Tunnicliffe, J., & Friedrich, H. (2019). SmartWood: Laboratory experiments for assessing the effectiveness of smart sensors for monitoring large wood movement behaviour. *Catena*, *182*, 104145. https://doi.org/10.1016/j.catena.2019.104145

Spreitzer, G., Tunnicliffe, J., & Friedrich, H. (2020a). Large wood (LW) 3D accumulation mapping and assessment using structure from motion photogrammetry in the laboratory. *Journal of Hydrology*, *581*, 124430. https://doi.org/10.1016/j.jhydrol.2019.124430

Spreitzer, G., Tunnicliffe, J., & Friedrich, H. (2020b). Porosity and volume assessments of large wood (LW) accumulations. *Geomorphology*, *358*, 107122. https://doi.org/10.1016/j.geomorph.2020.107122

Spreitzer, G., Tunnicliffe, J., & Friedrich, H. (2021). Effects of large wood (LW) blockage on bedload connectivity in the presence of a hydraulic structure. *Ecological Engineering*, *161*, 106156. https://doi.org/10.1016/j.ecoleng.2021.106156

Steeb, N., Rickenmann, D., Badoux, A., Rickli, C., & Waldner, P. (2017). Large wood recruitment processes and transported volumes in Swiss mountain streams during the extreme flood of August 2005. *Geomorphology*, *279*, 112–127. https://doi.org/10.1016/j.geomorph.2016.10.011

Wallerstein, N. P., Alonso, C. V., Bennett, S. J., & Thorne, C. R. (2001). Distorted Froude-scaled flume analysis of large woody debris. *Earth Surface Processes and Landforms*, *26*, 1265–1283. https://doi.org/10.1002/esp.271

Welber, M., Bertoldi, W., & Tubino, M. (2013). Wood dispersal in braided streams: Results from physical modeling. *Water Resources Research*, *49*, 7388–7400. https://doi.org/10.1002/2013WR014046

Wheaton, J. M., Brasington, J., Darby, S. E., Kasprak, A., Sear, D., & Vericat, D. (2013). Morphodynamic signatures of braiding mechanisms as expressed through change in sediment storage in a gravel-bed river. *Journal of Geophysical Research: Earth Surface*, *118*(2), 759–779. https://doi.org/10.1002/jgrf.20060

Wohl, E., Bolton, S., Cadol, D., Comiti, F., Goode, J. R., & Mao, L. (2012). A two end-member model of wood dynamics in headwater neotropical rivers. *Journal of Hydrology*, *462*(463), 67–76. https://doi.org/10.1016/j.jhydrol.2011.01.061

Wohl, E., Cenderelli, D. A., Dwire, K. A., Ryan-Burkett, S. E., Young, M. K., & Fausch, K. D. (2010). Large in-stream wood studies: A call for common metrics. *Earth Surface Processes and Landforms*, *35*, 618–625. https://doi.org/10.1002/esp.1966